ORIGINAL PAPER

APPLICATIONS OF PLASMA ELECTROLYTIC SATURATION TECHNIQUE IN THE FIELD OF NUCLEAR MATERIALS

VICTOR AUREL ANDREI[1,2], VIOREL MALINOVSCHI[2,3], CRISTIANA RADULESCU[1,4*], ION IONITA[1], GYULA TOROK[5], ELISABETA COACA[6], ALEXANDRU HORIA MARIN[6], GIZO BOKUCHAVA[7]

Manuscript received: 06.06.2018; Accepted paper: 18.12.2018;
Published online: 30.03.2019.

Abstract. *The aim of this study is to explore in-depth microstructural changes induced by Plasma Electrolytic Saturation nitriding and carburizing treatments applied to the AISI 304L steel. The obtained structures were characterized by X-Ray Diffraction, Metallography, X-ray Photoelectron Spectroscopy and Small Angle Neutron Scattering; an assessment of the results is presented.*

Keywords: *AISI 304L steel, Plasma Electrolytic Saturation, X-Ray Diffraction, X-ray Photoelectron Spectroscopy, Small Angle Neutron Scattering.*

1. INTRODUCTION

The purpose of controlled surface modification by surface engineering techniques can be to reduce corrosion, reduce friction energy loss, reduce wear, achieve thermal or electrical insulation, promote a certain type of interaction with various radiation fields. The problem of obtaining, characterizing and using materials with appropriate properties is very important in areas of activity involving advanced technologies - such as the nuclear field.

Numerous attempts have been made to develop nitriding and carburizing treatments based on electrochemical assisted plasma processing for a group of materials, including stainless steels. However, major uncertainties remain as regards the optimization, control and repeatability of processes, mainly because the scientific understanding of key processes in electrolytic plasma processing has long lasted behind empirical trials aimed at developing appropriate treatments.

Plasma Electrolysis (PE) is a generic term which is used to describe a variety of high voltage electrochemical processes occurring at an electrode-electrolyte interface, which include plasma electrolytic saturation [1]. Among the Plasma Electrolysis techniques, Plasma Electrolytic Saturation (PES) as Plasma Electrolytic Carburizing (PEC) and Plasma Electrolytic Nitriding (PEN), show excellent promise as cost-effective techniques for forming

[1] Valahia University of Targoviste, Institute of Multidisciplinary Research for Science and Technology, 130004 Targoviste, Romania. E-mail: andvic12@yahoo.com.
[2] ELSSA LABORATORY SRL, 110109 Pitesti, Romania.
[3] University of Pitesti, Faculty of Science, 110040 Pitesti, Romania.
[4] Valahia University of Targoviste, Faculty of Sciences and Arts, 130004 Targoviste, Romania.
Corresponding Author: Cristiana Radulescu; E-mail: radulescucristiana@yahoo.com.
[5] Budapest Neutron Centre, 1121 Budapest, Hungary.
[6] Institute for Nuclear Research, 115400 Mioveni, Romania.
[7] Joint Institute for Nuclear Research, Frank Laboratory of Neutron Physics, 141980 Dubna, Moscow Region, Russia.

surface layers of high tribological, corrosion and thermal barrier performance. Thermal diffusion effects during plasma electrolytic heating lead to electrolyte elemental diffusion into the surface of the electrode. However, further development of the plasma electrolytic processes to fulfil their potential in a broader range of surface engineering applications requires a better understanding of the physical and chemical background of the plasma phenomena occurring on the electrode during electrolysis. Thermal and diffusion processes, new plasma chemical reactions and macro-particle transportation (i.e. cataphoretic effects) become possible during electrolysis.

First step towards closing the knowledge gap between fundamental process understanding and coating characteristics is the characterization of the non-homogeneous surface structures developed by plasma-assisted electrochemical processes. Austenitic stainless steels AISI 304L and AISI 316L are widely used as structural materials in different fields [2-6]; in nuclear installations for example, CALANDRIA vessel and tubular plates in CANDU Nuclear Power plants are made from AISI 314L. In papers [7-9] were presented results regarding the obtaining and characterization of protective structures on martensitic and austenitic steels used as structural materials in the nuclear field; it has been shown that the steels treated by electrolytic plasma processing behave better at corrosion. In this paper the results of the characterization of surface structures developed on AISI 304L steel, by surface electrochemical treatment methods for improvement of the properties (corrosion resistance, hardness) are reported. The aim of this study is to explore in-depth microstructural changes induced by PES nitriding and carburizing treatments applied to the AISI 304L steel, correlating the information provided by surface sensitive investigation techniques (X-ray Photoelectron Spectroscopy - XPS, Grazing Incidence X-Ray Diffraction – GIXRD) with information obtained by SANS and XRD regarding the bulk of the material.

2. MATERIALS AND METHODS

AISI 304L stainless steel samples (10x10x1) mm^3, were manually grounded up to 1200 mesh SiC paper in order to achieve a fine finish with an average surface roughness of 0.35 mm, which minimizes the mechanical surface damage and allows a good adherence of a coated layer. Then the samples were cleaned with distilled water and ethanol before treatment. PES nitriding and carburizing treatments were applied to the AISI 304L steel samples using the experimental setting shown in Fig. 1. PES nitriding and carburizing treatments are described in Table1.

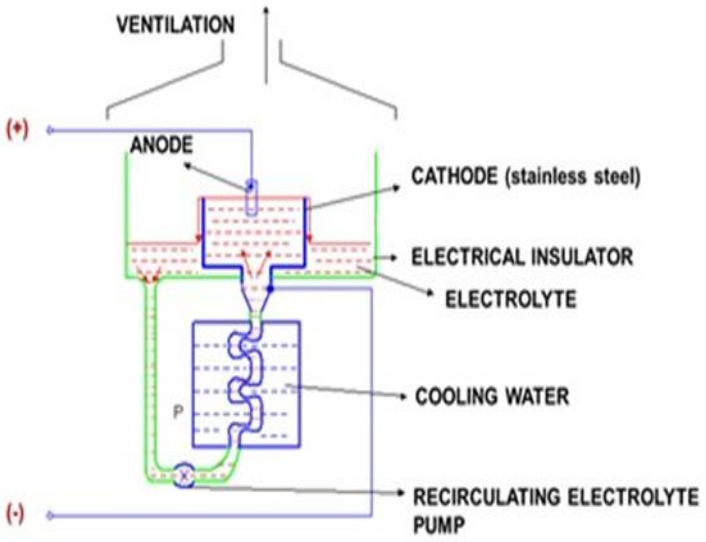

Figure 1. Experimental set-up for PES treatments.

Table 1. PES treatments.

Treatment	Sample code	Electrolyte composition	Experimental parameters
PES-N (nitriding)	304L-N	1.65 Kg NH_4Cl+ 1.5 Kg NH_4NO_3 + 15 Kg H_2O	U = 165 V, t = 3 min
PES-C (carburizing)	304L-C	1.5 Kg NH_4NO_3+ 1.2 l $C_3H_8O_3$ + 15 Kg H2O	U = 220V, I = 6A, t = 3min

The surfaces structures developed by PES treatments were investigated by optical microscopy, XRD, XPS and SANS.

For **Metallography**, the samples were cut into sections with the ISOMET 4000 device, and then packed into a copper foil and mounted in a thermoplastic raisin with the METAPRESS-A, METKOH covering press. After mounting, the sample was grinded and polished (120-2400 grained abrasive paper) with a BETA GRINDER-POLISHER-BUEHLER device. After polishing, samples were metallographic etched in order to evaluate the structure of the surface layer. The electrolytic etching was performed with oxalic acid 10%, 6V, 10-20 seconds.

X-ray diffraction (XRD) analysis of deposited layers was carried out using a Dron UM1 diffractometer. Qualitative phase analysis was established by recording the sample X-ray diffraction spectra in the following experimental conditions: Cu Kα radiation, accelerating voltage 40 kV and tube current 30 mA, the (2θ) scan range of 25°-100° with a step size [Δ(2θ)] of 0.05°, 10s step-time, Bragg-Brentano (θ-2θ) focusing scheme and a graphite monochromator in diffracted beam. The XRD diffraction peaks of standard 304L were collected in the above similar conditions. The crystallite sizes and micro-deformations of the polycrystalline Fe_3O_4 phase were estimated from the pure-specimen integral breadth of the (202) and (404) diffraction lines using multiple-order analysis. For an accurate microstructural analysis, instrumental broadening was taken into account by measuring the (110) and (220) reflection of LaB6 (SRM 660b) standard powder. For the analysis of the distribution of the layer deposited on the sample 304L-C of the polycrystalline phases, diffraction spectra or grazing incidence x-ray diffraction (GIXRD) were acquired in the angular range 34°-46° or for grazing angles of 1°, 1.5°, 2°, 3°, 4°, 5° and in Bragg-Brentano focusing (θ -2θ).

X ray Photoelectron Spectroscopy analysis (XPS) has been carried out in order to determine the surface composition and depth distribution of the elements. The ESCALAB 250 Electron Spectrometer has been used; X ray beam incident on the sample was focused on a spot with a diameter of 250 μm, and the energy resolution of the spectra was 0.65 eV. The Argon Ion Gun used for depth profiling was operated at 3 KV and 1 μA, the crater produced being a square with the 500 μm side. The depth profiling measurements using "Ball Cratering" technique was performed in order to evaluate the variation composition along the sample depth of tens of microns. "Ball Cratering" depth profiling analyzes was performed by XPS "line scan" along a line that starts from the surface and reaches the deepest point of the crater made by the ball sample [10].

Small Angle Neutron Scattering (SANS) measurements were performed on the SANS-diffractometer at Budapest Neutron Center. We have investigated the nanostructure of the surface layer affected as a result of plasma electrolysis processing as compared to base metal. We subtracted the SANS contribution of non-treated base sample using neutron beam (with wavelength λ=0.609nm, $\Delta\lambda/\lambda$= =0.25, beam diameter=8mm). The geometry of experiment is shown in Fig. 2.

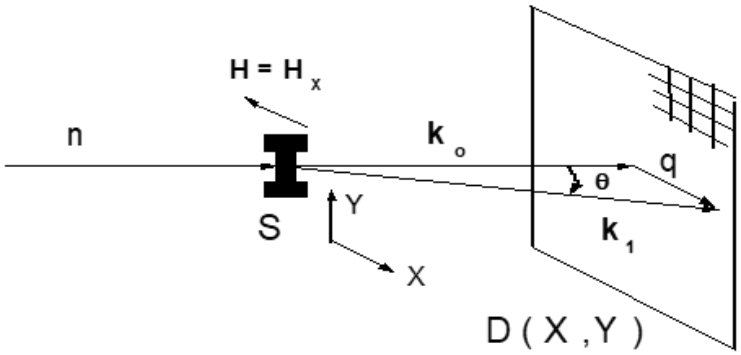

Figure 2. SANS-experiment: neutrons scattered from the sample (S) are registered in two-dimensional detector (D) where k_o, k_1 are the initial and final wave vectors of neutrons.

They were used in transmission geometry, packages of samples (10x10x1 mm^3) treated identically in order to increase the effective volume affected by treatment. The packages of samples of stainless steel with surface treatment were fixed and was applied a magnetic field 1.4T. We observed both the isotropic scattering pictures and anisotropic one.

3. RESULTS AND DISCUSSION

The applied treatments lead to the formation of adherent structures; the results of the metallographic study are shown in Fig. 3. As with conventional thermo-chemical diffusion treatments, the surface layers produced on steels by PEN/ C consist of two regions. Under the surface, treatment of PES-N and treatment of PES-C lead to the formation of a thin layer that can be assimilated to the inner diffusion area of thermo-chemical treatments (6-7 μm for treatment with PES-N, 35-40 μm for treatment of PES-C) [1].

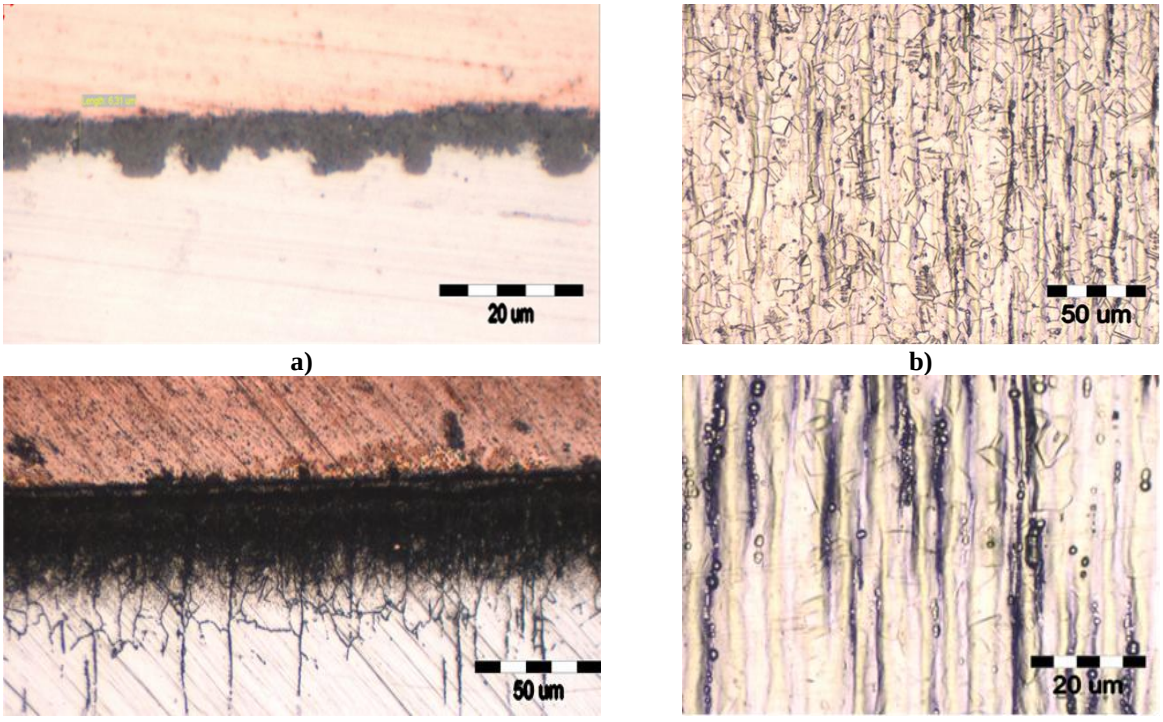

a) **b)**

c) **d)**

Figure 3. The results of the metallographic study: a) Sample 304L-N: Non-uniform surface layer of 6-7 μm; b) Sample 304L-N: substrate morphology; c) Sample 304L-C: Uniform surface layer of 35-40 μm; d) Sample 304L-C: substrate morphology.

The internal diffusion area of the perlite and retained austenite (with solids diffusion elements) gradually change into a non-sealed "white" outer layer, mainly formed of nitrides and iron carbides. The morphology of the substrate has an austenitic structure with parallel strings of carbides.

Qualitative phase analysis results (Fig. 4) of the recorded XRD patterns for sample 304L-N evidence the presence of polycrystalline phases Fe_3O_4 (JCPDS 89-2355), CrN (JCPDS 65-2899) and the substrate. Qualitative phase analysis results (Fig. 5a) of the recorded XRD patterns for sample 304L-C evidence the presence of polycrystalline phases Fe_3O_4 (JCPDS 89-2355), $(Cr,Fe)_7C_3$ (JCPDS 5-720), Fe_3C (JCPDS 89-2867) and the substrate.

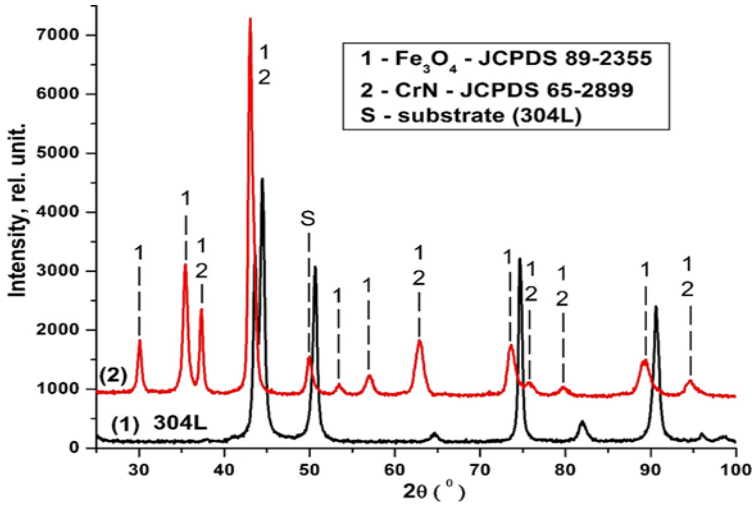

Figure 4. XRD patterns for 304L-N sample.

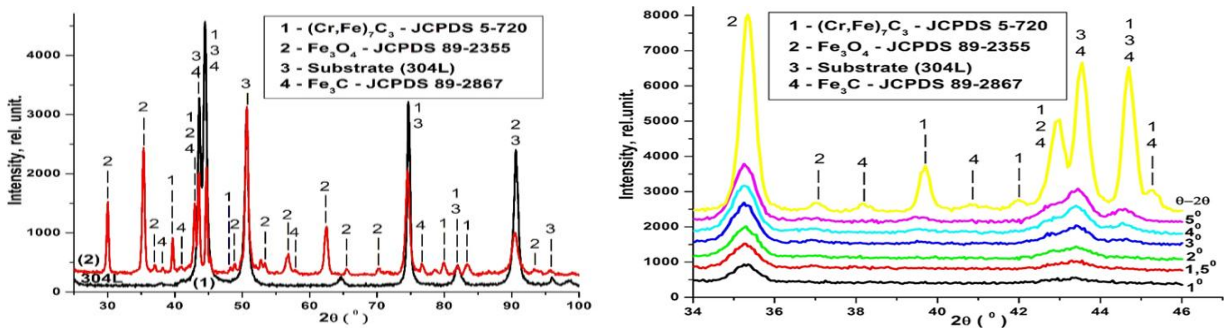

a) **b)**

Figure 5. XRD paterns for 304L-C sample: a) XRD patterns for 304L-C sample; b) GIXRD patterns for 304L-C sample

From the analysis of the overlapped diffraction spectra acquired in GIXRD configuration (Fig. 5a) it is observed that for the sliding angles $\alpha < 4^0$ XRD analysis in the layer only the polycrystalline phase Fe_3O_4 is present. For larger sliding angles, the polycrystalline phase $(Cr, Fe)_7C_3$ appears alongside this phase, and at even greater angles the Fe_3C phase appears. This phase distribution in the depth of the layer is confirmed by the metallographic analysis of the layer in the section (Fig. 3b) and the results of the XPS analysis (Fig. 8a-c).

Crystallite size and micro-strain calculations were assessed by approaching the size-strain analysis in terms of integral breadths. The physical profile of $K_{\alpha 1}$ singlet is described by Voigt function [12]**.** Multiple-order analysis assumes that the Cauchy component of the Voigt function gives the value of crystallite size and the Gaussian component gives the value of strain. Pure-specimen (physically) integral breadth of profile (β_f) produced by the convolution of a Cauchy profile with a Gaussian profile is expressed as follows:

$$\beta_f = \beta_{fG} \cdot \frac{\exp(-k^2)}{1-erfc(k)} \qquad k = \frac{\beta_{fC}}{\sqrt{\pi} \cdot \beta_{fG}}$$

where β_{fC} and β_{fG} are the breadth of Cauchy and Gauss functions [13].

If size and strain broadening is present simultaneously then the crystallite size and strain are obtained from the integral breadth of physical profiles for the first and second order diffraction lines (β_{f1} si β_{f2}). The size of the spherical assumed crystallite and the root mean square strain (RMSS) are:

$$\langle D \rangle_V = \frac{8}{3} \frac{\pi}{\beta_{fC}} \qquad \text{and} \qquad \langle \varepsilon^2 \rangle^{\frac{1}{2}} = (2\pi)^{-\frac{3}{2}} \cdot d_{HKL}^{(1)} \cdot \beta_{fG}^{(1)},$$

where $d_{HKL}^{(1)}$ is the interplanar spacing related to the first order reflection (m=1). Inasmuch as $\prec D \succ_V$ depends only on β_{fC}, it results that β_{fC} does not depend on the diffraction order, namely $\beta_{fC}^{(1)} = \beta_{fC}^{(m)}$, m=2, 3, 4... $\beta_{fG}^{(m)} = m \cdot \beta_{fG}^{(1)}$, since $d_{HKL}^{(1)} = m \cdot d_{HKL}^{(m)}$.

The integral breadth of physical profiles (β_{f1} and β_{f2}) for the (202) and (404) diffraction lines of Fe_3O_4 were estimated by Fourier analysis of experimental and instrumental profiles. Calculated values of crystallite sizes and micro-strains are shown in Table 2.

Table 2. Crystallite size and micro-strain (root mean square strain) values calculated from physical integral breadth of Fe_3O_4 (202) and (404) diffraction lines.

Sample code	$\langle D \rangle$ [nm]	$\varepsilon_0 = \sqrt{\langle \varepsilon^2 \rangle}$
304L_C	62 ± 3	$(2.8 \pm 0.1) \cdot 10^{-3}$
304L_N	41 ± 2	$(4.7 \pm 0.1) \cdot 10^{-3}$

The survey spectra obtained after the PES-N and PES-C treatments before the argon ion bombardment are shown in Fig. 6 and highlight the presence of common superficial contaminants (C, O, N, Na, and Ca). One can estimate for our experiment a sputtering rate of 0.8 nm / s [10].

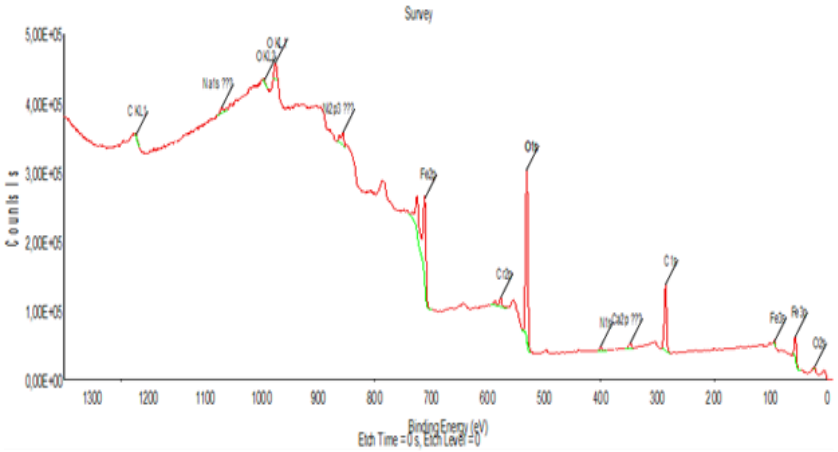

Element	Atomic %
Fe	10
Cr	1
Ni	1.2
O	44
C	40
N	2
Na	1
Ca	0.8

a)

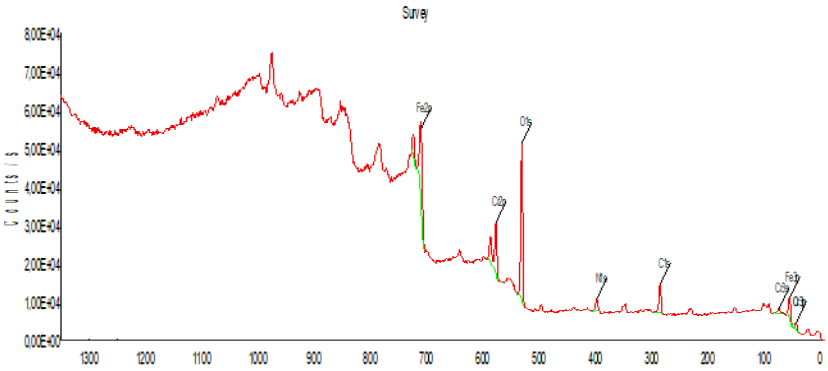

Element	Atomic %
Fe	11
Cr	8
Ni	2
O	53
C	26

b)

Figure 6. The survey spectra of 304L-N and 304C before Argon ion etching: a) 304L-N sample; b) 304-C sample.

Fig. 7a shows the disappearance of carbon contamination peak by removing a 20 nm layer by sputtering with argon ions on 304L-N sample. Figs. 7b-c show that after removal of the first N-adsorbed monolayer, N is chemically bound to Cr.

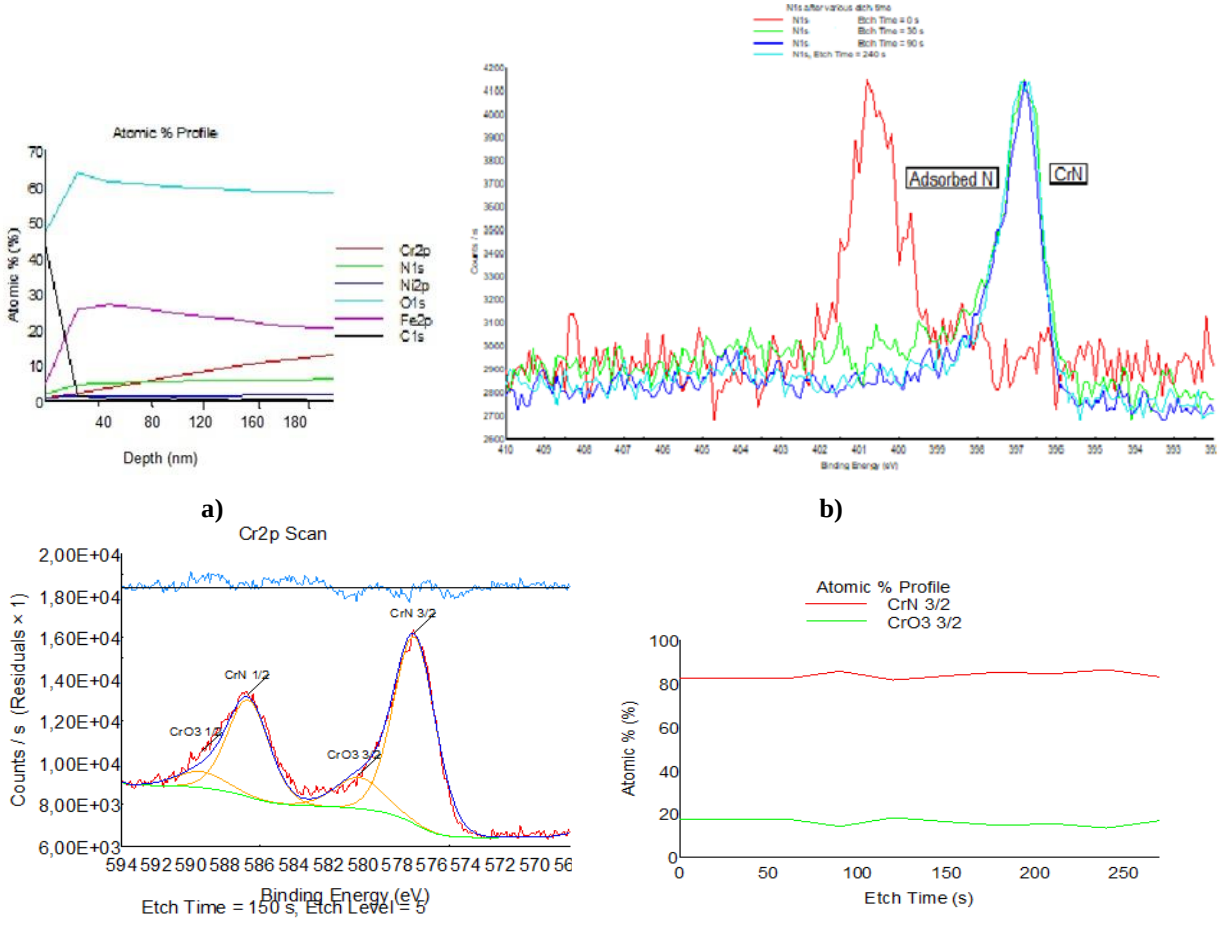

Figure 7. XPS results for 304L-N sample: a) Depth profiling; b) Evolution of spectrum for N1s at different times of etching; c) Deconvolution of Cr 2p doublet; d) Distribution of the atomic percent of the chemical states of Cr in the depth.

XRD and XPS analyzes confirm the presence of Fe_3O_4 and CrN in surface layer; up to a depth of 40 nm the concentration of Cr and N atoms increases then stabilizes. The deconvolution of the Cr2p doublet is difficult because Cr2p peak has significantly split spin-orbit components (Δ=9.3eV) and a satellite feature of the Cr2p3/2 peak overlaps the Cr2p1/2

component in Cr_2O_3. XPS spectrum of Cr2p energy region (Fig. 8c) shows two contributions at BE of 575.2 eV assigned to Cr_7C_3 and 577.3 eV assigned to Cr_2O_3 according to results reported in [11].

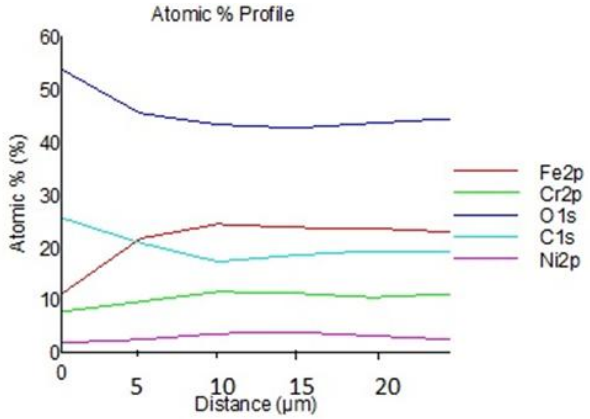

a)

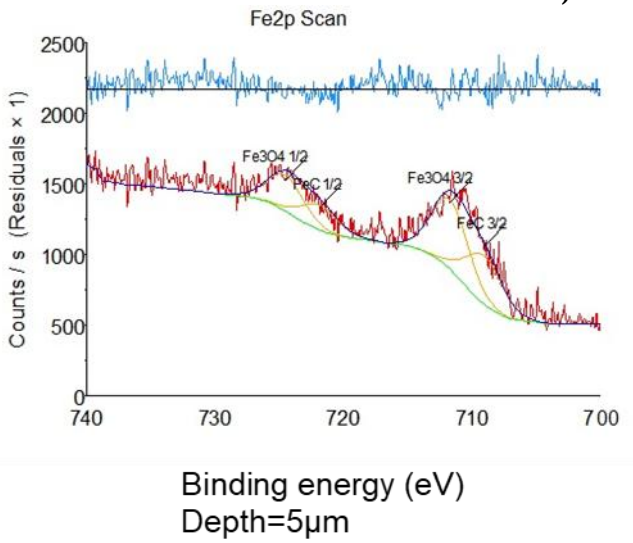

Chemical state	Binding Energy of Fe2p3/2 [eV]
Fe_3O_4	711.4
Fe3C	708.2

b)

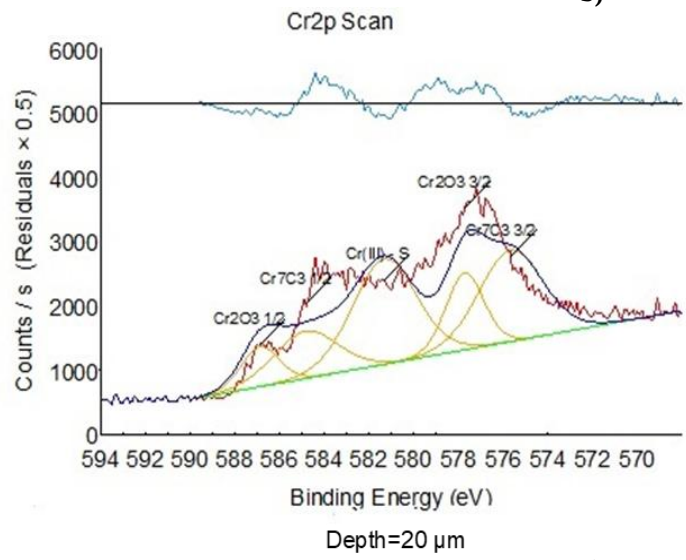

Chemical state	Binding Energy of Cr2p3/2 [eV]
Cr_7C_3	575.2
Cr_2O_3	577.3

c)

Figure 8. XPS results for 304L-C sample: a) Depth profiling (Ball Cratering); b) b) Deconvolution of Fe2p doublet; c) Deconvolution of Cr 2p doublet.

SANS data analyses were done by Bersans program package separating the possible magnetic contribution from nuclear one. The scattering intensity of nuclear part is fitted by a sum of Guinier function and a fractal part: Y = A + I1 * exp(-R2q 2/3) + F * qC, where the first part is a simplest approximation of scatterers and the second term represents the density fluctuations at the border of precipitates (usually that is formed by diffusion processes, so most probably the shape is DLA fractal). The fitted parameters are: R-averaged radius of scattering centre, F - fractal part (inter-granular area), C - dimension of fractal structure. The results of SANS analysis of 304L samples are presented in Fig. 9 and Table 3.

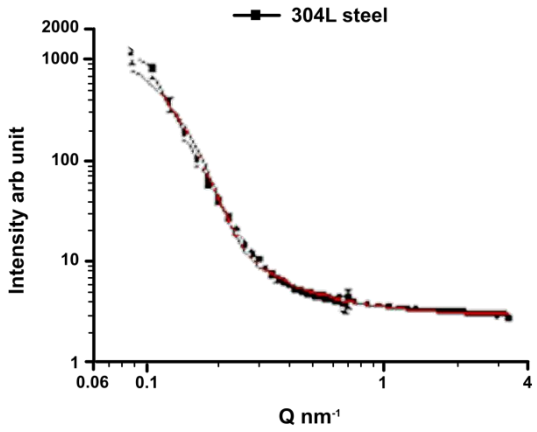

a)

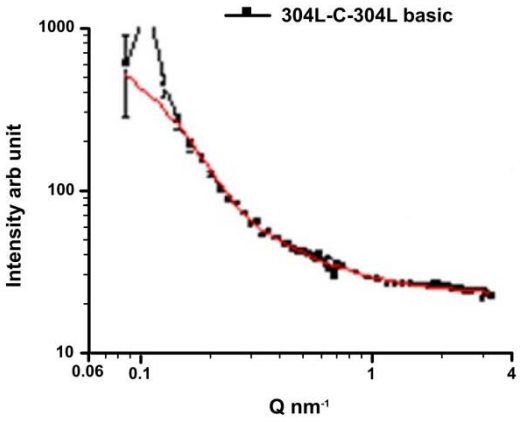

b)

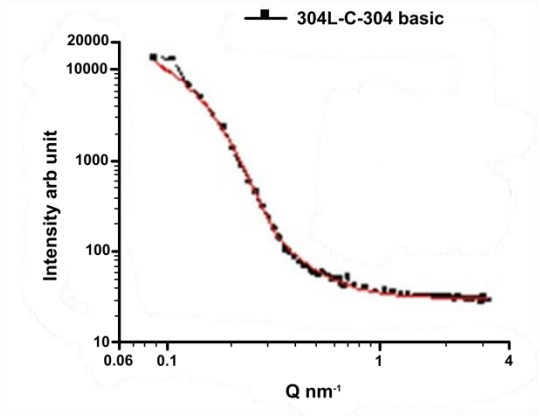

c)

Figure 9. SANS results: a) Fit for sample Basic 304 steel, Nuclear scattering; b) Fit for sample difference of 304L-N –Basic 304 steel, Nuclear scattering; c) Fit for sample difference of 304L-C –Basic 304 steel, Nuclear scattering.

Table 3. SANS results (values for Gyration radius are expressed in nm).

Sample / treatment	Background (A) / Intensity (I1) Gyration radius (R)	Fractality measure (F) dimension (C)
304L basic	A =2.963 ± 0.033 I1 =1528.63 ± 0 R =17.14 ± 0.24	F= 0.538 ± 0.061 C = -1.965 ± 0.121
304L-N-304L basic	A= 22.882 ± 0.465 I1= 366.67 ± 352.46 R= 12.78 ± 2.59	F = 7.0339 ± 0.712 C = -1.449 ± 0.117
304L-C-304L basic	A =29.91 ± 0.345 I1 =12676.9 ± 951.0 R =13.49 ± 0.22	F = 4.557 ± 0.623 C = -2.789 ± 0.153

In sample 304L-N the averaged size of scattering particles 2R=25.6 nm with volume fractal structure close to the lamellar one, and their surface fractal structure is close to the lamellar form with sharp border. In sample 304L-C the averaged size of scattering particles 2R=27 nm. The fractal part which represents the area of inter-granular matter is increased what is the other side of dissolution process [11]. The original fractal structure is a volume fractal with dimension of a hairy structure. At treated area the fractal dimension is corresponding to a volume fractal dense and smooth, the ratio of fractal part is growing [14].

Optimization in plasma electrolysis treatments involves understanding the changes in structure and composition both in thin layers (thickness of tens of Å) using surface science techniques (e.g. XPS and AES) and in layers with thicknesses of tens of microns. This study sought to identify micro and nano - structural changes in layers with thicknesses of tens of microns. It is aimed to identify the microstructural transformations at crystal cell level, eventually the segregation of alloying elements as result of plasma electrolysis treatment. The SANS measurement can exactly show at what circumstances are beginning the phase transformation/segregation process, so we can optimize the applied treatment.

4. CONCLUSION

Plasma Electrolytic Nitriding treatment leads to the rapid (3 minutes) production of a superficial film composed of Fe_3O_4 and CrN, with a thickness of 6-7 microns. Plasma Electrolytic Carburizing treatment leads to the rapid (3 min.) production of a superficial film composed of Fe_3O_4, Fe_3C and $(Cr, Fe)_7C_3$, with a thickness of 35-40 microns. Using surface science techniques (XPS, GIXRD) and complementary techniques that inform about bulk, it can understand changes in structure and composition in both thin layers (thickness tens of Å) and in layers with thicknesses of tens of microns. SANS measurements provides information about the nanostructure of the surface layer affected as a result of plasma electrolysis processing as compared to base metal when using, in transmission geometry, packages of samples treated identically in order to increase the effective volume mofified by treatment.

REFERENCES

[1] Yerokhin A.L. et al., *Surf. Coat. Technol.*, **122**, 73, 1999.
[2] Despa, V. et al., *J. Sci. Arts*, **4**(41), 839, 2017.
[3] Rusanescu, C.O. et al.,*Optoelectron. Adv. Mat. Rap. Comm.*, **7**(11-12), 947, 2013.
[4] Rusanescu, C.O. et al., *Rev. de Chimie (Bucharest)*, **66**(5), 754, 2015.
[5] Poinescu, A. et al., *J. Sci. Arts*, **1**(42), 275, 2018.
[6] Anghelina, F.V. et al., *Appl.Surf.Sci.*, **285**(15), 65, 2013.
[7] Andrei, V. et al., *New Applications of Micro and Nanotechnology*, Ed. Academiei Romane, Bucharest, 2009.
[8] Ducu, C. et al., *Proceedings of E-MRS*, 2221, 2007.
[9] Poinescu, A.A. et al., *Rev. de Chimie (Bucharest)*, **65**(10), 1245, 2014.
[10] Watts, J.F., Wolstenholme, J., *An Introduction to Surface Analysis by XPS and AES*, John Wiley & Sons Ltd., Chichester, 2003.
[11] Castillejo, F.E. et al., *Surf. Coat. Technol.*, **254**, 104, 2014.
[12] Langford, J.I., *J. Appl. Crystallogr.*, **11**, 10, 1978.
[13] Schoening, F.R.L., *Acta Crystallogr.*, **18**, 975, 1965.
[14] IAEA-TECDOC-1486, *Small angle neutron scattering*, Report AIEA, 2006.